Naval Research Laboratory

Stennis Space Center, MS 39529-5004

NRL/MR/7180--14-9540

Evidence for High Nonlinearity in Sandy Sediment Using an Air Gun Source

B. Edward McDonald

Acoustic Systems Branch
Acoustics Division

Steve Stanic

Acoustic Simulation, Measurements, and Tactics Branch
Acoustics Division

July 3, 2014

REPORT DOCUMENTATION PAGE

Form Approved
OMB No. 0704-0188

1. REPORT DATE *(DD-MM-YYYY)*	**2. REPORT TYPE**	**3. DATES COVERED** *(From - To)*
03-07-2014	Memorandum Report	June 2010

4. TITLE AND SUBTITLE

Evidence for High Nonlinearity in Sandy Sediment Using an Air Gun Source

5a. CONTRACT NUMBER

5b. GRANT NUMBER

5c. PROGRAM ELEMENT NUMBER

6. AUTHOR(S)

B. Edward McDonald* and Steve Stanic*

5d. PROJECT NUMBER

5e. TASK NUMBER

5f. WORK UNIT NUMBER
71-6378-01

7. PERFORMING ORGANIZATION NAME(S) AND ADDRESS(ES)

Naval Research Laboratory
Acoustics Division
Stennis Space Center, MS 39529-5004

8. PERFORMING ORGANIZATION REPORT NUMBER

NRL/MR/7180--14-9540

9. SPONSORING / MONITORING AGENCY NAME(S) AND ADDRESS(ES)

Office of Naval Research
One Liberty Center
875 North Randolph Street, Suite 1425
Arlington, VA 22203-1995

10. SPONSOR / MONITOR'S ACRONYM(S)

ONR

11. SPONSOR / MONITOR'S REPORT NUMBER(S)

12. DISTRIBUTION / AVAILABILITY STATEMENT

Approved for public release; distribution is unlimited.

13. SUPPLEMENTARY NOTES

*The research was performed during the authors' previous employment with the Naval Research Laboratory.

14. ABSTRACT

An airgun source near the seafloor was used to initiate weakly nonlinear acoustic waves that propagated down into a sandy sediment. Below the airgun at an appropriate offset were two 12-element vertical arrays to monitor the waves' evolution from 10 cm above the seafloor to a depth of 1 meter in the seafloor. Analysis of the resulting waveforms gave values of log-pressure increase with time that are too large to be explained by linear theory, or even fluid-like nonlinearity. We investigate the possibility that nonlinearities inherent to granular media are responsible for the observations.

15. SUBJECT TERMS

Acoustics
Nonlinear sediment interaction

16. SECURITY CLASSIFICATION OF:			**17. LIMITATION OF ABSTRACT**	**18. NUMBER OF PAGES**	**19a. NAME OF RESPONSIBLE PERSON**
a. REPORT	**b. ABSTRACT**	**c. THIS PAGE**			Steve Stanic
Unclassified Unlimited	Unclassified Unlimited	Unclassified Unlimited	Unclassified Unlimited	31	**19b. TELEPHONE NUMBER** *(include area code)* (228) 688-5235

Standard Form 298 (Rev. 8-98)
Prescribed by ANSI Std. Z39.18

I. Introduction

In this paper we will (1) describe an experiment we performed to measure the propagation of weakly nonlinear waves into sandy sediment, then (2) develop a method for tracking wavefronts in the initial rise of a weakly nonlinear wave, and (3) use the method to extract nonlinear parameters as a function of overpressure.

During 14-17 June 2010, we carried out an experiment at the Naval Surface Warfare Center, Panama City FL, to observe the development of pressure- time series versus depth in the seafloor of waves from a weakly nonlinear airgun source. Our motivation was the lack of experimental studies of nonlinear wave propagation into marine sediments. Prior to the expermient, we searched open literature for information on this subject, and contacted many in the nonlinear acoustics community for help locating experimental data. We found primarily references to papers by Muir[1], Bjorno[2], Hovem[3] in the 1970's. Muir made the case for examining *dynamic* nonlinearity, whereas engineering studies had carried out *static* studies with hydraulic presses using dried sediment samples. Bjorno[2] carried out an experiment with saturated sediment, but these were done by sending a *linear* acoustic wave through a vessel subjected to a constant pressure load. This is not the same as subjecting a saturated sediment to a single nonlinear impulse, in which fluid and granular sediment both are subjected to sudden impulsive stress increases. The analysis of Bjorno's result by Hovem[3] using Biot theory and fluid nonlinearity gave results consistent with unstressed sand grains in stress- bearing water[4]. Namely, the analysis gave results consistent with a nonlinear parameter in the range 5 to 7, where nonlinear parameter is defined as

$$\beta = 1 + \frac{1}{2}\frac{\rho_0}{c_0^2}\frac{\partial^2 p}{\partial \rho^2}\bigg|_0 = 1 + \frac{\partial \log c}{\partial \log \rho}\bigg|_0 \tag{1}$$

where ρ is density, p is pressure (or more generally normal stress), c is sound speed, and

Manuscript approved June 5, 2014.

subscript zero means evaluation in the ambient state.

In 2007 a Korean group reported[5] a value of the nonlinear parameter for saturated sandy sediment equal to 73, from a laboratory experiment measuring second harmonic generation from a constant frequency source. This nonlinearity was attributed to gas bubbles rather than granular contacts. Insonification with a linear source is closer to a static, rather than dynamic, test. Part of our motivation for the 2010 airgun experment was to determine pressure - time series *dynamically* in hopes of observing possible departures from fluid - like behavior. In the category of fluid - like behavior, we include water containing microbubbles, since air and water are both fluids. The nonlinearity coefficient of bubbly water as a function of gas volume fraction begins at about 3.5 for pure water, then reaches a maximum of 5000 for a gas volume fraction 6×10^{-5}, then falls to 1.2 for pure air.

The most likely non- fluid mechanism affecting nonlinear propagation in sediments is the Hertz force[6,7] between sediment grains in contact. The Hertz force is proportional to $\epsilon^{3/2}$, where ϵ is the strain rate. In the limit of small strain between dry grains, $\epsilon \propto \rho'$ and $p' \propto \rho'^{3/2}$, where primes denote small but finite perturbations to ambient values. In this limit, the nonlinearity coefficient from (1) for a dry granular frame with constant numbers of contact points between grains is proportional to $\rho'^{-1/2}$, which diverges in the limit of small stress. The question we will examine is whether the normal stress in a real marine sediment exhibits non- fluid behavior of the nonlinearity coefficent at low stress.

II. Experimental Setup

We conducted the experiment in the Gulf of Mexico at the Naval Surface Warfare Center, Panama City FL, during 14 - 17 June 2010, at a location (30.092750N 85.711466666W)

where the bathymetry was flat and depth was 10m. Figure 1 is a schematic of the experimental configuration. The experiments were conducted in the Gulf of Mexico in an area 2 miles east of the entrance to St. Andrews Bay. A 30m long support craft was anchored about a mile off shore. Divers from NRL used a water jet system to bury a pair of 12-element, 1m long hydrophone arrays. The top element of each array was positioned just above the water-sediment interface and an in-water hydrophone was positioned 2m above the water-sediment interface.

An air gun was mounted on an aluminum frame 0.86m above the seafloor. The vertical arrays were placed in the sandy sediment, each offset in two directions from directly below the air gun ports. From the spot directly below the ports, a point 5 feet (1.52m) to the north was marked, from which east and west offsets of 2 feet (0.61m) were marked to sink the vertical arrays (with water jets) into the sediment. The horizontal displacement was made to avoid shadowing of the array hydrophones by their casings and by neighboring hydrophones. The horizontal offset of each array from the point below the air gun was thus 1.64 m (Figure 2). Throughout this paper we use sound speed in water 1537.4m/s from CTD data taken very near our site in June 2003 (Figure 3).

The air gun had a maximum source level of 208 - 226 dB@1m, with bandwidth 20Hz - 8kHz. The gun's air chamber of 20 in^3 was charged with pressures from 140 psi to 2000 psi (14MPa). The 2000 psi pressure was used during most of the experiments. A series of high-energy broad band pulses (1 to 8 kHz) with a rep. rate of .03 Hz were transmitted into the sediment and pressure- time series were recorded as a function of depth by each of the hydrophone arrays.

One of the arrays was monitored in real time aboard our work boat, while the second

array was recorded continuously in a bottom mounted pressure vessel. The results presented here are from the bottom mounted pressure vessel, since the real time system was subjected to continuous calibration changes.

The reason for conducting an at- sea experiment versus a tank experiment with glass beads was to sample a real seafloor environment; assemblies of glass beads can have artificial symmetries (*e.g.* hexagonal close packing) with preferred propagation directions not found in nature. Tanks are also plagued with wall reflections.

III. Theory

The theoretical approach to be taken is as follows: First, we investigate the behavior of a broadband *linear* source near the seafloor as a baseline. Second, we examine the ability of fluid nonlinearity to steepen propagating wavefronts and compare to experimental results. Third, we investigate the ability of granular nonlinearity to explain the experimental results.

A. Linear Theory

For the linear analysis, a point source near a fluid- fluid seafloor interface is resolved into plane waves, and then plane wave Rayleigh reflection and transmission coefficients are converted to cylindrical values by the appropriate azimuthal integrals in the water and the seafloor. This approach has been used in examining acoustic transmission from water to air[8]. Results from linear theory are compared with experimental results. The discrepancies with linear theory are examined with weakly nonlinear theory for fluid - like media which is also found inadequate. Although shear waves are initiated in the seafloor, they are quite weak in the near field (small depths) due partly to high porosity. Also, under stress, shear waves may lead to media failure (slips).

In unbounded water, the pressure field of a point source with time dependence $\exp(-i\omega t)$ normalized to pressure p_0 at radius r_0 and its spatial Fourier transform are given by[8]

$$p = p_0 r_0 \frac{\exp(ik_w r)}{r} = \frac{p_0 r_0}{2\pi^2} \int \exp(i\mathbf{q}\cdot\mathbf{r}) \Big[(q^2 - k_w^2)^{-1} + i\frac{\pi}{2k_w}\delta(q - k_w) \Big] d^3\mathbf{q} \qquad (2)$$

where $k_w = \omega/c_w$, c_w is sound speed in water, and $q = |\mathbf{q}|$. Values for the experiment were $c_w = 1537.4 m/s$, and sound speed in the bottom $c_b = 1711 m/s$. The density of the seafloor relative to water was 2.0.

We adopt a Cartesian coordinate system and place the point source at $(x, y, z) = (0, 0, z_s)$, where $z_s > 0$ is height above the seafloor, and $z = 0$ at the seafloor.

Carrying out the q_z integration in (2), the acoustic field without the seafloor interface is

$$p = \frac{p_0 r_0}{2\pi^2} \int d^2\mathbf{q}_\perp \exp(i\mathbf{q}_\perp \cdot \mathbf{r}) F(z, q_\perp), \qquad (3)$$

$$F(z, q_\perp) = \begin{cases} i\pi u^{-1} \exp i|z - z_s|u, & q_\perp^2 < k_w^2 \\ \\ \pi u^{-1} \exp -|z - z_s|u, & q_\perp^2 > k_w^2 \end{cases} \qquad (4)$$

where $u = \sqrt{|k_w^2 - q_\perp^2|}$ and $\mathbf{q}_\perp = (q_x, q_y)$.

1. Addition of the Seafloor Interface

A seafloor interface at $z = 0$ is added by use of appropriate plane wave reflection coefficients. Snell's law dictates constancy of the horizontal wavenumber $\mathbf{q}_\perp$ across the interface. Three horizontal wavenumber regimes are considered in both the water column and the seafloor. We retain evanescent waves, since results will be calculated in the near field. Separate expressions for the water column and seafloor follow. Let $k_b = \omega/c_b$, where c_b is the sound speed in the seafloor, and define absolute value vertical wavenumbers

$$u = \sqrt{|k_w^2 - q_\perp^2|} = q_{wz}, \quad s = \sqrt{|k_b^2 - q_\perp^2|} = q_{bz} \tag{5}$$

1. $z > 0$ (Water Column)

$$q_\perp^2 < k_b^2 : \qquad F(z, q_\perp) = i\tfrac{\pi}{u}\left(\exp i|z_s - z|u + R_0 \exp i(z_s + z)u\right) \tag{6}$$

$$R_0 = \frac{u - \alpha s}{u + \alpha s} \quad \alpha = \frac{\rho_w}{\rho_b} \tag{7}$$

$$k_b^2 < q_\perp^2 < k_w^2 : \qquad F(z, q_\perp) = i\tfrac{\pi}{u}\left(\exp i|z_s - z|u + R_1 \exp i(z_s + z)u\right) \tag{8}$$

$$R_1 = \frac{u - i\alpha s}{u + i\alpha s} \tag{9}$$

$$q_\perp^2 > k_w^2 : \qquad F(z, q_\perp) = \tfrac{\pi}{u}\left(\exp -|z_s - z|u + R_0 \exp -(z_s + z)u\right) \tag{10}$$

---

2. $z < 0$ (In the Sea Floor)

$$q_\perp^2 < k_b^2 : \qquad F(z, q_\perp) = i\tfrac{\pi}{u}(1 + R_0) \exp i(z_s u - sz) \tag{11}$$

$$k_b^2 < q_\perp^2 < k_w^2 : \qquad F(z, q_\perp) = i\tfrac{\pi}{u}(1 + R_1) \exp i z_s u \ \exp sz \tag{12}$$

$$q_\perp^2 > k_w^2 : \qquad F(z, q_\perp) = \tfrac{\pi}{u}(1 + R_0) \exp(-z_s u + sz) \tag{13}$$

Keeping $\mathbf{r}$ fixed, we carry out the horizontal wavenumber integral in (3) using $d^2\mathbf{q}_\perp = dq_\perp \cdot q_\perp d\phi$,where ϕ is the azimuthal angle (dropping subscript $\perp$ from $q_\perp$ and $r_\perp$ for notational simplicity):

$$\begin{aligned} p &= \frac{p_0 r_0}{2\pi^2} \int d^2q \exp(i\mathbf{q} \cdot \mathbf{r}) F(z, q) = \frac{p_0 r_0}{2\pi^2} \int_0^\infty dq F(z, q) \int_0^{2\pi} q d\phi \exp iqr \cos\phi \\ &= \frac{p_0 r_0}{\pi} \int_0^\infty J_0(qr) F(z, q) q dq, \end{aligned} \tag{14}$$

where J_0 is the zero order Bessel function. Then (14) becomes

$$\begin{aligned}\frac{p}{p_0 r_0} &= i\int_0^{k_b} \frac{1+R_0}{u} \exp i(z_s u - sz)\ J_0(qr)\ q\ dq \\ &+ i\int_{k_b}^{k_w} \frac{1+R_1}{u} \exp iz_s u\ \exp sz\ J_0(qr)\ q\ dq \\ &+ \int_{k_w}^{\infty} \frac{1+R_2}{u} \exp(-z_s u + sz)\ J_0(qr)\ q\ dq\end{aligned} \tag{15}$$

Reflection coefficients R_i for the three wavenumber regions of (15) may be expressed as

$$\begin{aligned}\frac{1+R_0}{u} &= \frac{2}{u+\alpha\sqrt{u^2-u_1^2}}, \qquad u_1^2 = k_w^2 - k_b^2 \\ \frac{1+R_1}{u} &= \frac{2}{u+i\alpha\sqrt{u^2-u_1^2}}, \qquad \alpha = \frac{\rho_w}{\rho_b} \\ \frac{1+R_2}{u} &= \frac{2}{u+\alpha\sqrt{u^2+u_1^2}}\end{aligned} \tag{16}$$

In (16), the expressions involving R_0 and R_1 are restatements of (7) and (9), while that for R_2 is a restatement of R_1 for high wavenumber $q > k_w$.

2. Amplitude, Phase, and Nearly Spherical Waves

The airgun pulses as received on the arrays had characteristic durations of order 2ms, with peak frequency approximately 600Hz. Numerical synthesis of these pulses was performed with integrals over a frequency range 1-1800 Hz, using environmental values quoted after (2). We will show from evaluation of (15-16) that in the near field (including the near seafloor), amplitude is very closely related to phase throughout the relevant frequency range. We will also find that phase and amplitude surfaces for downward propagating waves remain very nearly spherical in both water column and seafloor.

Our basis of comparison for the experimental time series will be first, the constancy of $\partial \log p/\partial t$ on a constant phase surface for a linear wave in a homogeneous fluid, and second the near constancy of $\partial \log p/\partial t$ on the numerical results from (15) across the seafloor.

For a linear spherical pulse in a homogeneous medium, the pressure from a point source may be expressed as

$$p(r,t) = f(r-ct)/r \tag{17}$$

In a coordinate system fixed in the medium, (17) gives

$$\partial \log p/\partial t = -cf'(r-ct)/f(r-ct). \tag{18}$$

On a constant phase surface $r - ct = const$, $\partial \log p/\partial t$ by (18) remains constant.

When evaluating a complex pressure field such as (15) at a single frequency, phase surfaces are well defined. When a broadband impulsive wave is received on a hydrophone, one has only amplitude to deal with. Even if one could assume the sound speed perfectly known, one would have to deal with the fact that phase surfaces move at speed c, but in the near field, ray paths for computing phase are only a high frequency approximation. We

have chosen an empirical approach, in which linear benchmark calculations synthesized a broadband pulse by integrating (15) over frequencies, and evaluated pressure- time series at the hydrophone locations.

a. Amplitude as Proxy of Phase

The experimental pulses as received on the arrays had characteristic timescales of order 2ms, with spectal peak at approximately 600Hz. Numerical construction of a baseline linear solution for comparison with these pulses was performed integrating over a frequency range 1-1800 Hz. We will show from evaluation of (15) that in the near field, amplitude is very closely correlated with phase throughout the relevant frequency range, even after propagation through the seafloor.

The advantage of amplitude tracking versus wavefront (phase) tracking for a broadband pulse in the near field is summarized as follows: (1) In order to track a wavefront, one has to calculate $ds/dt = c$ along a ray, with s the arc length along the ray. Rays are a high frequency approximation, while the farthest phone from the source is less than three wavelengths for $c_w = 1537.4m/s$ at 1800Hz. (2) If one were to attempt wavefront tracking, then environmental uncertainties in c_b could be mistaken as results of nonlinearity. Values of c_b are available for selected cores taken in past experiments, but amplitude is measured *in situ* as part of the experiment, so is more faithful to the array location.

Our baseline linear solution is taken for a source whose amplitude referenced to 1m is one cycle of a 600Hz sinusiod:

$$p(t, 1m) = \frac{p_1}{2}\big(1 + \cos(\pi - \omega_0 t)\big), \qquad 0 \le t \le 2\pi/\omega_0, \tag{19}$$

and $p(t, 1m) = 0$ outside this range. Here $\omega_0 = 2\pi \cdot 600Hz$, and p_1 is an arbitrary reference

pressure at 1m. The form of (19) was chosen to approximate the initial rise of measured pressure pulses.

Figure 4 summarizes simulated peak pressures on the array elements from the numerical evaluation of (15), normalized to the peak value 1m from the source. Peak pressures follow an approximate power law $r^{-1.15}$, where r is the slant range from the source to array elements. The use of slant range is justified by the fact that the fractional difference in ray path length and slant range over the array was a maximum of 0.003 at phone 11, 10cm below the seafloor.

The fractional power law is not an indication of nonlinearity, but reflects that the transmission coefficient across the seafloor increases with horizontal distance out to the array location. Each array element receives energy that has crossed the seafloor in slightly different regions with different transmission coefficients. Critical incidence (grazing angle 26°) occured just past the array at a horizontal range 1.76m.

We examined contour plots of the wave synthesized from (15-16) as it progressed down into the sediment, and found the wavefronts surprisingly spherical. Wavefront sphericity is illustrated by the correlation between the slant range from source to points in the sediment, and the phase of the individual frequency components of the wave from (15-16) over a range 1 - 1800Hz: For two complex quantities A and B, define the volume correlation coefficient

$$C(A,B) \equiv \frac{|\int A \cdot B dv|^2}{|\int A^2 dv \cdot \int B^2 dv|} \tag{20}$$

where the integration volume is a cylinder with vertical axis extending from the seafloor directly below the source to a depth of 1m, and out to the radius of 1.64m where the array is located.

In Figure 5 we show the differential correlation $1-C(\phi,r)$ *vs* frequency f, represented as $k_w z_s/\pi = 2fz_s/c_w$ where $z_s = .86m$, ϕ is the phase of the complex solution (15-16), and r is the slant range from the source to a point in the integration volume. For most of the frequency range, $1-C(\phi,r) < 10^{-4}$. This quantifies the near sphericity of the synthesized wave from (15-16).

Further confirmation of the closeness of the wave to a spherical wave is shown in Figure 6, which gives $1 - C(\phi \cdot A, 1)$, where A is the amplitude of the wave. (The correlation with unity is chosen for convenience; any nonzero constant gives the same result). For most of the frequency range, $1 - C(\phi \cdot A, 1) < 10^{-3}$. This shows that the product of amplitude and phase is very nearly constant over the frequency range 1 - 1800Hz. For a linear spherical wave in a homogenious medium, the correlation is exact for all frequencies.

IV. Experimental Results

Figure 7 shows a typical pressure - time series display for airgun shot number 15, with pressure represented as hydrophone voltage, with conversion factor 10kPa/Volt. The amplitude markers (dots) are positioned as follows: The seafloor phone (number 11) is marked at a desired value in the useful range of the phone (in Fig. 5, 1.75v). The useful range for hydrophone voltage is above zero, and less than the clipping value 3.5v. Above 1.75v, however, detailed analysis of the waveforms revealed sampling artifacts possibly due to overloading of the hydrophone. Calculations were made for marker values at phone 11 from 0.2v to 1.75v. Phone 10 was erratic throughout the experiment, and is not included in any of the results.

Time series from other phones are marked at values determined from the empirical

power law $r^{-1.15}$ as shown in Fig. 4. These markers are intended to show a point on the same wavefront as that passing through the marker for phone 11, including effects of spreading and variation of transmission coefficient with range along the seafloor.

a. Ability of Amplitude Tracking to Probe the Seafloor

Before considering nonlinearities, we will demonstrate that the amplitude tracking proposed above gives reasonable results for sound speed in the seafloor. The motivation for amplitude tracking is to use the wave itself as a probe, instead of assuming a known value of c_b. If c_b is imposed as known, then any early or late arrivals could easily be confused with the nonlinear dependence of c with pressure.

We use data from the first day of testing; the second day was plagued with equipment problems. We took 72 shots, exemplified by Fig. 7, using the amplitude markers as described above. We propose that the wavefronts carrying the amplitude markers originate at a common point at time t_0. Since we are in the near field, we compared ray paths obeying Snell's law (Fig. 2), and slant- range paths with no deflection at the seafloor in order to test sensitivity to propagation paths, and found insignificant differences.

Taking the arrival time of the amplitude marker at phone n (Fig. 2) to be t_n, one has

$$t_n = t_0 + r_{n,w}/c_w + r_{n,b}/c_b \tag{21}$$

where $r_{n,(w,b)}$ denotes the propagation path length in water and seafloor. Evaluating $t_1 - t_{11}$ eliminates the unknown t_0. With path lengths known from either rays obeying Snell's law, or slant ranges, and taking c_w known, one finds an expression which yields the path averaged c_b (the path to phone 11 is entirely in the water column):

$$t_1 - t_{11} = (r_{1,w} - r_{11,w})/c_w + r_{1,b}/c_b \tag{22}$$

The result for c_b is shown in Figure 8 for 72 ray paths obeying Snell's law. (On this series of 86 shots, the first 14 were engineering tests done at low pressure with the airgun hanging off the workboat.) The results for slant range paths with no deflection at the seafloor gives an increase in c_b which amounts to a shift by about the size of the plotting character. To be more specific, rays obeying Snell's law give average c_b and standard deviation (1725.6 $\pm$ 10.1)m/s, while slant range paths with no deflection at the seafloor give (1730.0 $\pm$ 10.5)m/s. The Snell's law result is slightly higher than one standard deviation from the assumed value 1711m/s. We note that the both the assumed seafloor sound speed of 1711m/s and the wavefront tracking value 1725.6 m/s fall within the range 1708-1771m/s found $in-situ$[9] during Sax99.

b. Time Series in the Seafloor

Figure 9 summarizes data for shots 15 - 86 taken on the first day of the expermient. (The second day was plagued by equipment failures.) The data are values of $\partial \log p/\partial t$ evaluated at the amplitude markers as shown in Fig. 7. Also shown is the linear benchmark solution computed from eq. (14) using the same amplitude marking method used in the experimental curves. It is apparent that the linear benchmark value of $\partial \log p/\partial t$ remains nearly constant as the wave propagates through the seafloor. The measured values, however, are low in the water column (phone 12), and increase significantly as the wave enters the seafloor and continue to increase as the wave propagates to a depth of one meter in the seafloor.

c. Effects of Fluid-Like Nonlinearity

Can the quadratic nonlinearity of a fluid explain the increase of $\partial \log p/\partial t$ with propagation path in the sediment? To answer this, we will give a comparison with the nonlinear

acoustic model NPE[10]. NPE is a time domain formulation for the evolution of a weakly nonlinear wave following a wavefront through a nearly homogeneous medium. The NPE for spherical waves is:

$$D_t p' = -\beta \frac{p'}{\rho c} \partial_r p' - c\frac{p'}{r}, \qquad D_t \equiv \partial_t + c\partial_r, \tag{23}$$

where D_t is the time derivative in a wave- following frame moving at speed c. When the nonlinear term is dropped, linear spherical waves of the form (17) satisfy (23). From (23) we find

$$D_t \log p' = -\frac{\beta}{\rho c} \partial_r p' - \frac{c}{r} \tag{24}$$

The time derivative fixed in the medium is $\partial_t = D_t - c\partial_r$, and for homogeneous media, ∂_t commutes with D_t. Then (24) yields

$$D_t \partial_t \log p' = -\frac{\beta}{\rho c} \partial_r \partial_t p' \qquad = \frac{\beta}{\rho c} \partial_t \left(\frac{1}{c} \partial_t p' + \frac{p'}{r} \right), \tag{25}$$

where the second equality is a result of the linear portion of p' being of the form (17). In the linear approximation, the wave- following range derivative is $c^{-1} D_t$. Eq. (25) may now be integrated along a wave- following radial to give

$$\partial_t \log p'(r_1) - \partial_t \log p'(r_{11}) = \overline{\beta} \int_{r_{11}}^{r_1} \frac{1}{\rho c^2} \left(\frac{1}{c} \partial_t^2 p' + \frac{\partial_t p'}{r} \right) dr, \tag{26}$$

where $\overline{\beta}$ is defined as a path- averaged value (β may vary with range and overpressure). Carrying out the integral in (26) using shot- average values of $\partial_t \log p'$ for data shown in Fig. 9 yields $\overline{\beta} = 5.56 \times 10^3$. In (26), r_1 and r_{11} are radials to the deepest hydrophone and the seafloor hydrophone (Fig. 2), with respective values 2.480m and 1.853m for two of the three cases given in Table 1 below.

The sensitivity of our estimate $\overline{\beta}$ to the amplitude tracking scheme was tested as follows. The data shown in Fig. 9 were analyzed using the empirical power law $p \propto 1/r^{1.15}$ as in Fig. 4. When the power law index was varied between 1.00 (marker points moved to higher values) and 1.35 (marker points moved to lower values), the values for $\overline{\beta}$ varied between 4.74×10^3 and 1.16×10^4 respectively.

Keeping the power law fixed at $1/r^{1.15}$, we found the following values of effective nonlinear coefficient with amplitude:

TABLE 1. Variation of $\overline{\beta}$ with Amplitude.

p_{11}(v)	$\overline{\beta}$
0.2	4.16×10^4
0.531	1.41×10^4
1.75	5.56×10^3

The entries in Table 1 resulted from shots with the airgun mounted in the aluminum frame as discussed above, except for the one for $p_{11} = 0.531$v. This value was taken from a low pressure engineering test in which the airgun was suspended by a cable 20 feet above the seafloor.

Our amplitude tracking method suggests a high nonlinearity coefficient $\overline{\beta}$ which decreases with increased amplitude. Fluids including air and water are sometimes represented with a polytropic equation of state $p \propto \rho^\gamma + const.$ Such an equation of state gives a constant β as long as the polytropic index γ is constant. High values of nonlinearity coefficient may be realized in bubbly fluids, and also in granular media. The nonlinearity coefficient

for bubbly water reaches a maximum of about 5000 for air volume fraction 6×10^{-5}, while values for dry clay sediments[11] fall in the approximate range 100 to 1000. We cannot rule out the possibility that gas bubbles and granular media nonlinearities are both related to our results.

If the normal stress p' is partially due to Hertzian contacts[6] between grains, β would vary with the inverse square root of amplitude in the limit of small strain (see discussion at the end of Sec. I). If one takes the upper and lower values of p_{11} in Table 1 to define a power law, one finds $\overline{\beta} \propto {p_{11}}^{-0.928}$, which falls off faster than the inverse square root variation for Hertzian contacts.

V. Discussion

Our experiment examined pressure- time series in sandy sediment for weakly nonlinear waves resulting from airgun shots in the water column. Calculations from linear theory for a plane fluid- fluid surface in the range 1 - 1800Hz resulted in waves remaining nearly spherical across the seafloor, despite the change in density and sound speed at the seafloor (Figs. 3-4). This is probably related to the fact that our hydrophones were in the near field of the source. We employed an empirical amplitude marking scheme motivated by Fig. 4 to track equivalent wavefronts down the hydrophone array. As shown in Fig. 8, amplitude marking gives a sound speed for the sediment close to the assumed value 1711 m/s and within the range of $in - situ$ measurements[9].

As shown in Fig. 9, the log- pressure time derivative for a linear pulse benchmark calculated from eq. (14), using the same amplitude marking scheme as for the data, remains nearly constant with depth, while the experimental values averaged over 72 shots increases significantly with depth as the wave progresses down the array. This indicates

that the experimental results are not in agreement with linear theory. The high values for the nonlinearity coefficient in our analysis (Table 1) are suggestive of both bubbly media and granular media. The general decrease of the nonlinearity coefficient with increased overpressure seen in Table 1 is qualitatively suggestive of Hertzian contacts between grains.

Comparison of our results in Table 1 with others for granular and porous media nonlinearity is as follows. As we mentioned earlier, Hovem's analysis[3] of an experiment on saturated but unstressed marine sediment implies nonlinear parameters in the range 5 to 7. A Korean experiment[5] using second harmonic generation gave a value 73, which was attributed to gas bubbles. Ostrovsky[11] quotes values of 800 for marble, $10^2 - 10^3$ for clay marine sediments, and 10^4 or more for granite and other solids. Ostrovsky[11] also presents a theory and experimental results for a quadratic nonlinearity involving fluid flow in micropores. The nonlinear parameter for the pore flow mechanism in a plastic medium was found to reach a peak value of 10^5 for porosity equal to 6.6×10^{-6}. The nonlinear parameter falls rapidly with increasing porosity, attaining a value 370 for porosity 2.6×10^{-3}. The porosity in the upper seafloor at a location northwest of our area was found in the Sax99 experiment to be approximately 0.38. At this high value, the pore flow mechanism is quite weak. To our knowlege, none of the other nonlinear mechanisms discussed here predicts the decrease of nonlinearity coefficient with increased amplitude.

We recommend further laboratory and field experiments to do the following: (1) A null experiment with source and array suspended in water. (2) An independent investigation into our amplitude tracking scheme for a solitary broadband nonlinear pulse. (3) A field experiment done in conjunction with *in situ* measurements for sound speed, density, and gas volume fraction.

ACKNOWLEDGMENT

Work supported by the Office of Naval Research. We thank Jeff Schindall, Geoff Edelmann and Michael Nicholas of the Naval Research Laboratory for their efforts in the design and maintenance of the hydrophone array and recording apparatus.

REFERENCES

[1] T. Muir, "Nonlinear acoustics and its role in the sedimentary geophysics of the sea," *Physics of Sound in Marine Sediments*, (edited by Loyd Hampton, Plenum, New York, 1974) pp. 241-291.

[2] L. Bjorno, "Finite amplitude wave propagation through water- saturated marine sediments," Acustica **38**, 195 - 200 (1977).

[3] J. Hovem, "The nonlinearity parameter of saturated marine sediments," *J. Acoust. Soc. Am.* **66**, 1463 - 1467 (1979).

[4] B. E. McDonald, "Modeling acoustic nonlinearities in marine sediments," *J. Acoust. Soc. Am.* **116**, 2549 (2004).

[5] B. N. Kim, K. I., S. W. Yoon, B. K. Choi, I. N. Didenkulov, "Nonlinear parameter estimation in water-saturated sandy sediment with difference frequency acoustic waves," (presented at a meeting of the Russian Acoustical Society, Nizhny Novgorod, 2004), pp. 119-123, available at URL http://spravka.akin.ru/Docs/Rao/Ses15/F31.PDF/ (Last viewed 11/04/2013).

[6] L. D. Landau and E. M. Lifschitz, *Theory of Elasticity* (Addison- Wesley, Reading, MA, 1959), pp. 26-31.

[7] B. E. McDonald, "Stability of self-similar plane shocks with hertzian nonlinearity," *J. Acoust. Soc. Am.* **120**, 3503 - 3508 (2006).

[8] B. E. McDonald and D. C. Calvo, "Enhanced sound transmission from water to air at low frequencies," *J. Acoust. Soc. Am.* **122**, 3159 - 3161 (2007).

[9] M. D. Richardson, "Overview of SAX99: Environmental Considerations," *et al, IEEE*

J. Ocean. Eng., **26**, 26-53 (2001).

[10] B. E. McDonald and W. A. Kuperman, "Time domain formulation for pulse propagation including nonlinear behavior at a caustic," *J. Acoust. Soc. Am.* **81**, 1406 - 1417 (1987).

[11] L. A. Ostrovsky, "Wave processes in media with strong acoustic nonlinearity," *J. Acoust. Soc. Am.* **90**, 3332-3337 (1991).

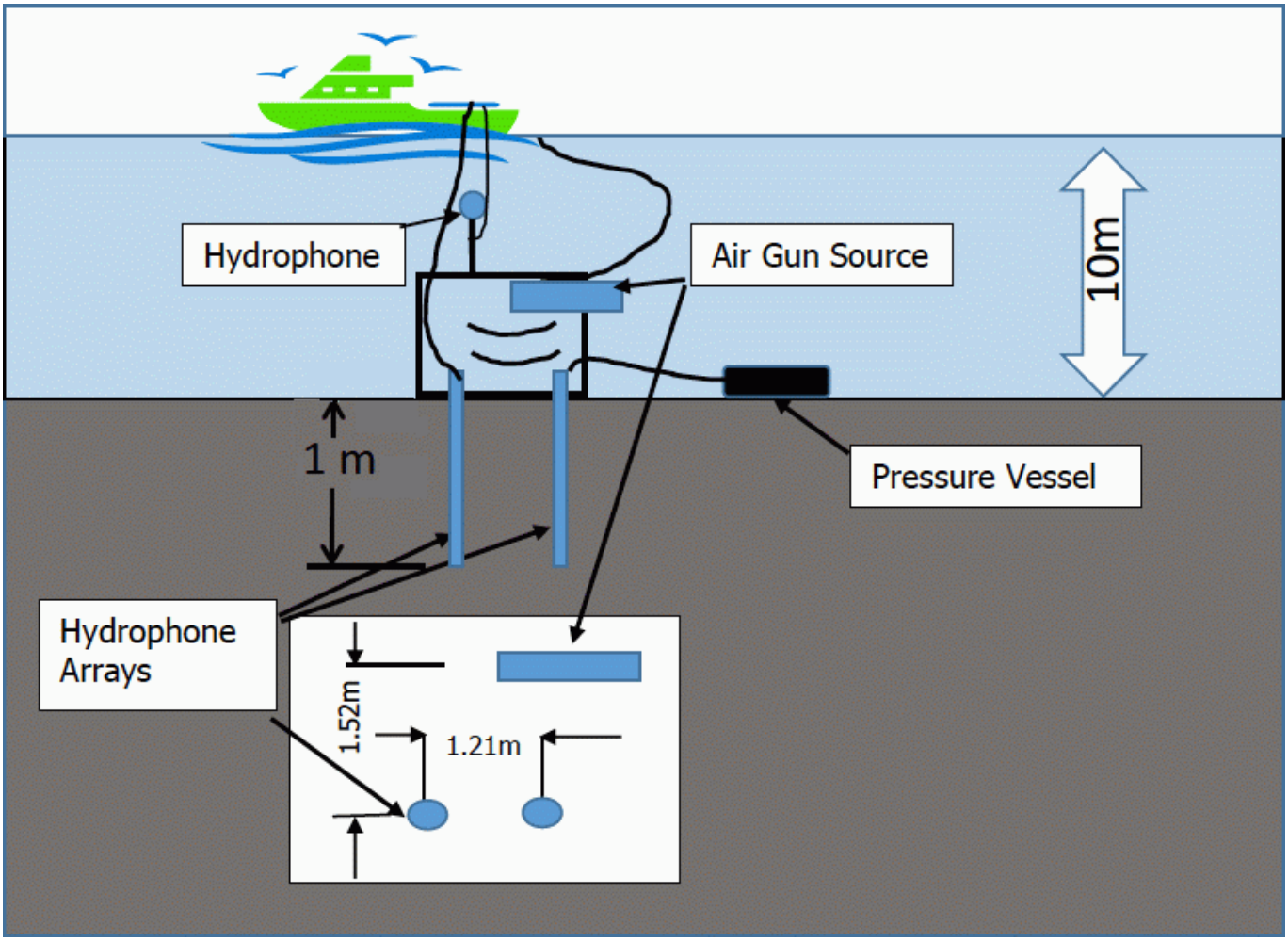

Figure 1. Experimental configuration. Front view above; Top view below.

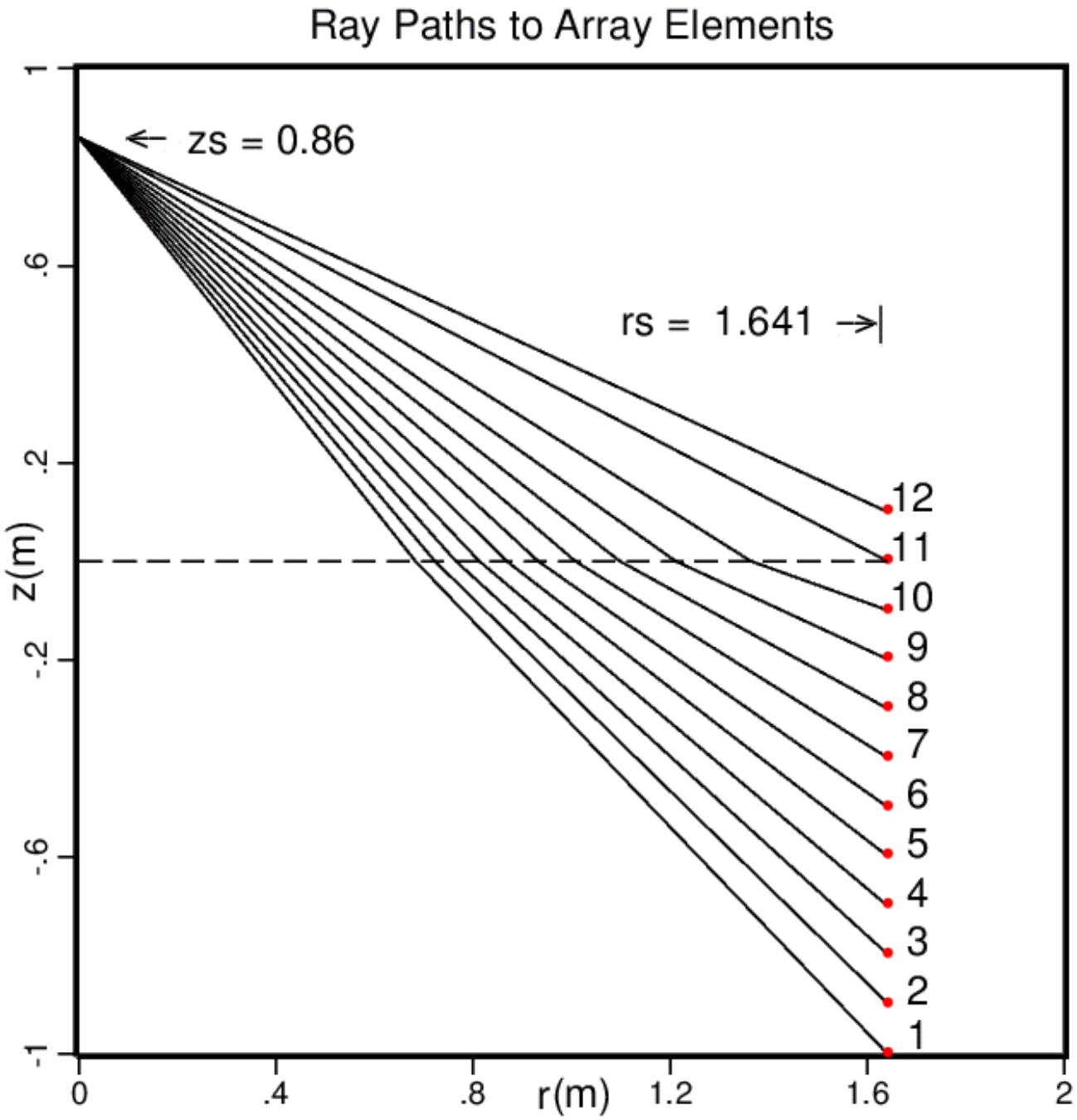

Figure 2. Schematic of airgun source above the seafloor and ray paths from Snell's law to each of the array elements.

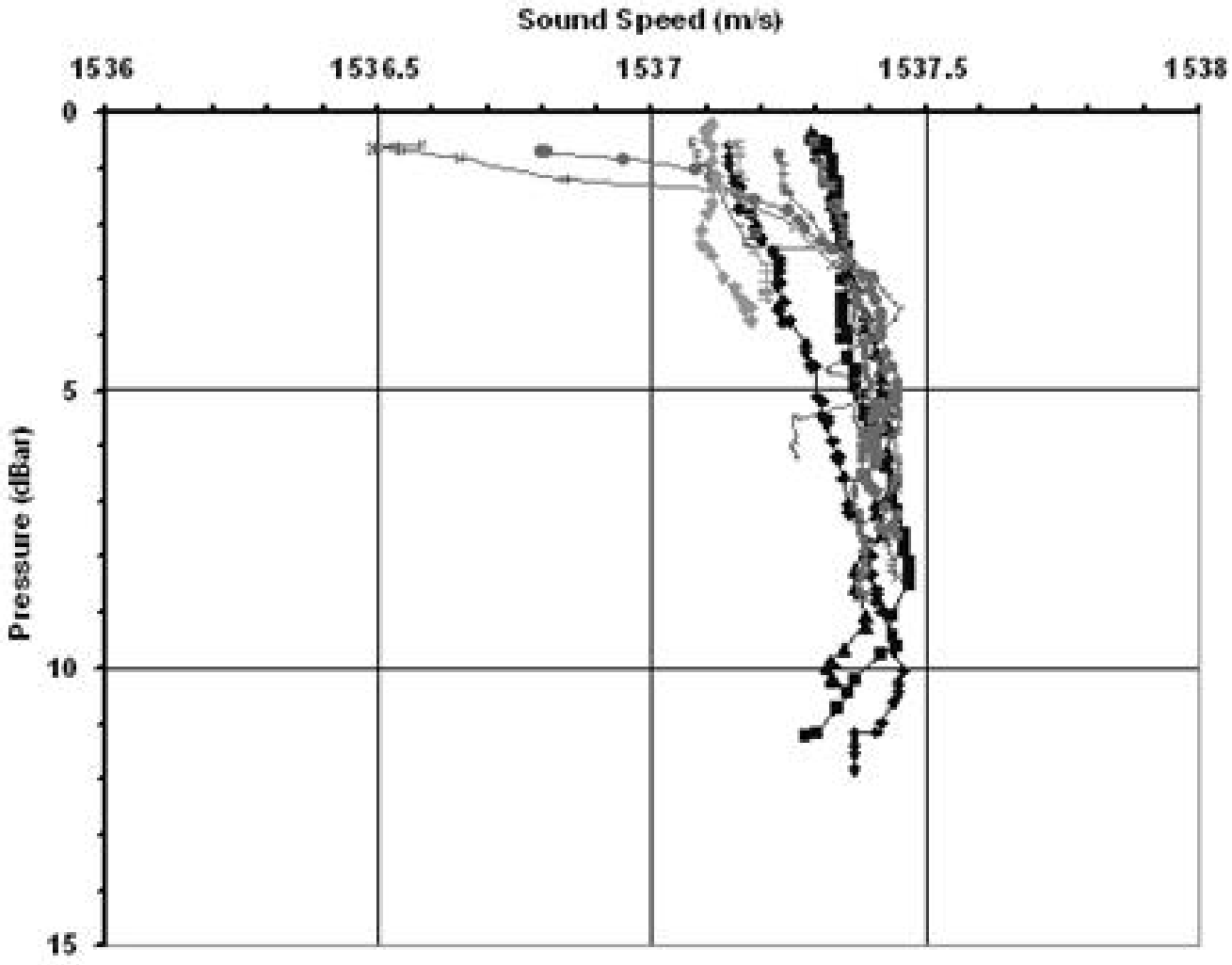

Figure 3. Sound speed profiles taken in our area in June 2003.

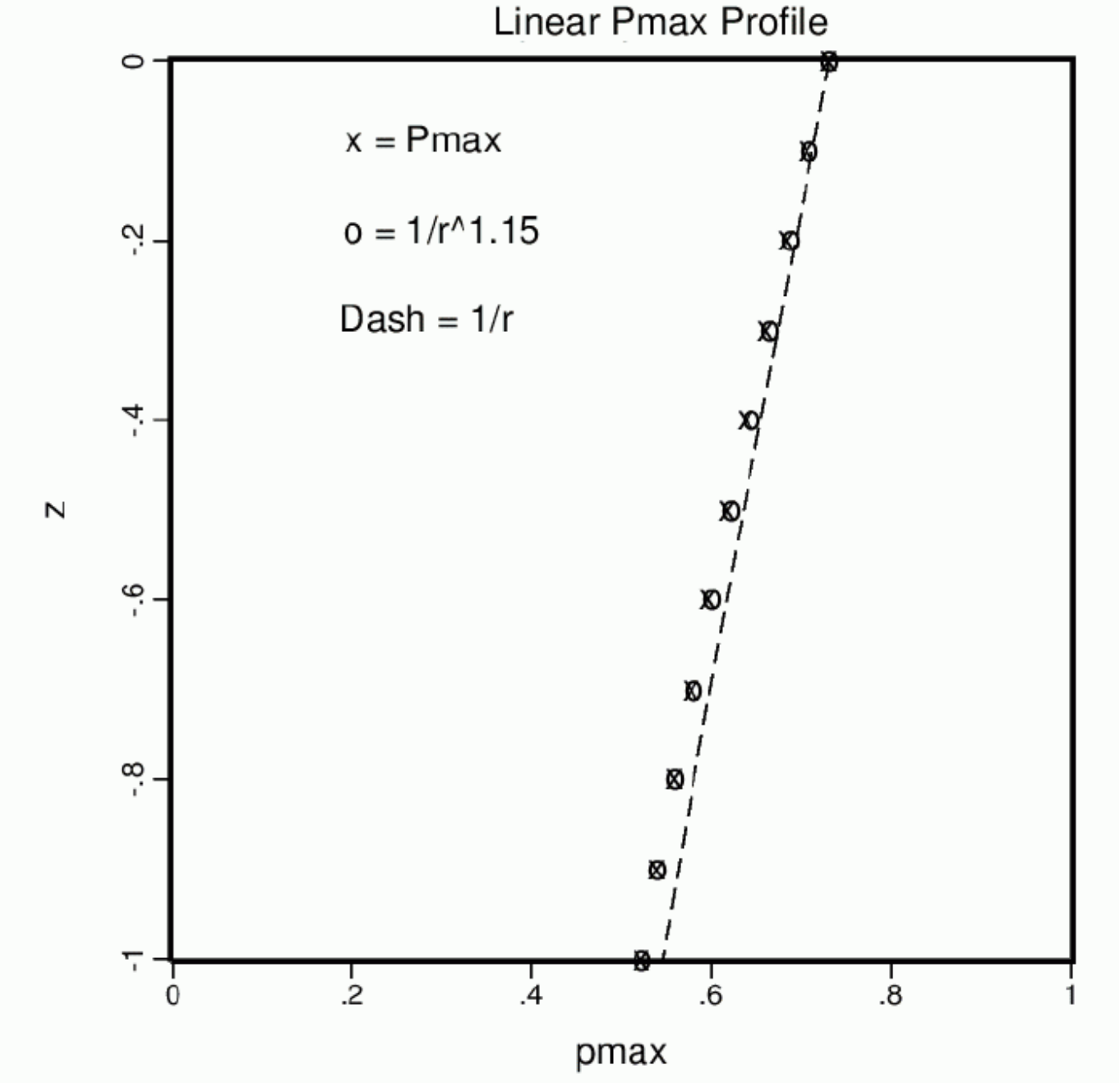

Figure 4. x: Peak pressures from linear field of eqs. (15-16) for a 600Hz source at the airgun location, normalized to the pressure at 1m. o: Empirical power law approximating the result. Dash: 1/r (slant range) dependence.

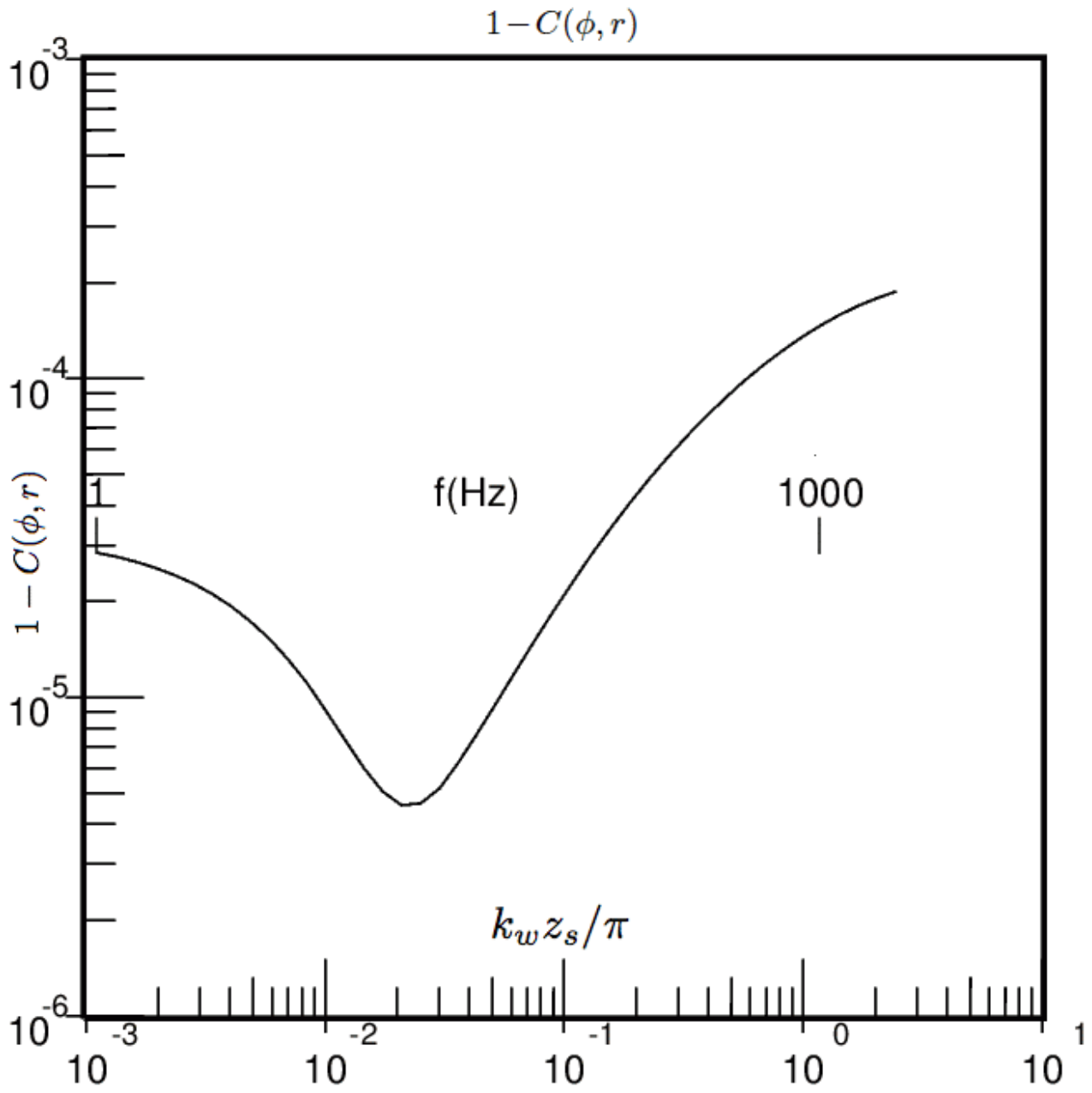

Figure 5. Differential correlation between the phase of a sinusoidal wave (including seafloor interface) and the slant range integrated over the cylindrical volume centered on the point below the source, extending out to the array range. The abscissa is the dimensionless wavenumber in the water, and expressed also as frequency (1 - 1800Hz).

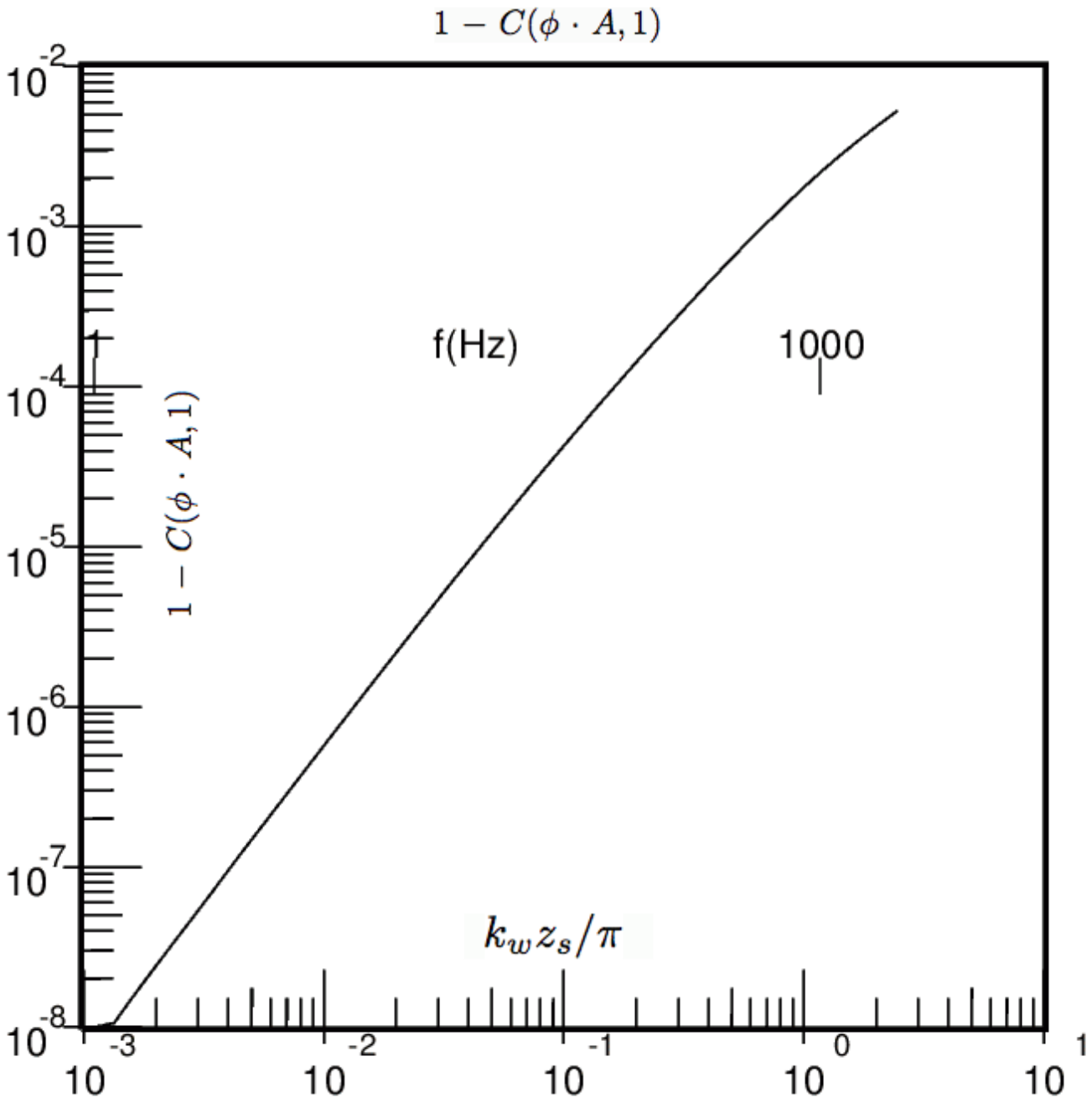

Figure 6. Differential correlation between the phase- amplitude product of a sinusoidal wave, and a constant value. Other details are as in Fig. 5.

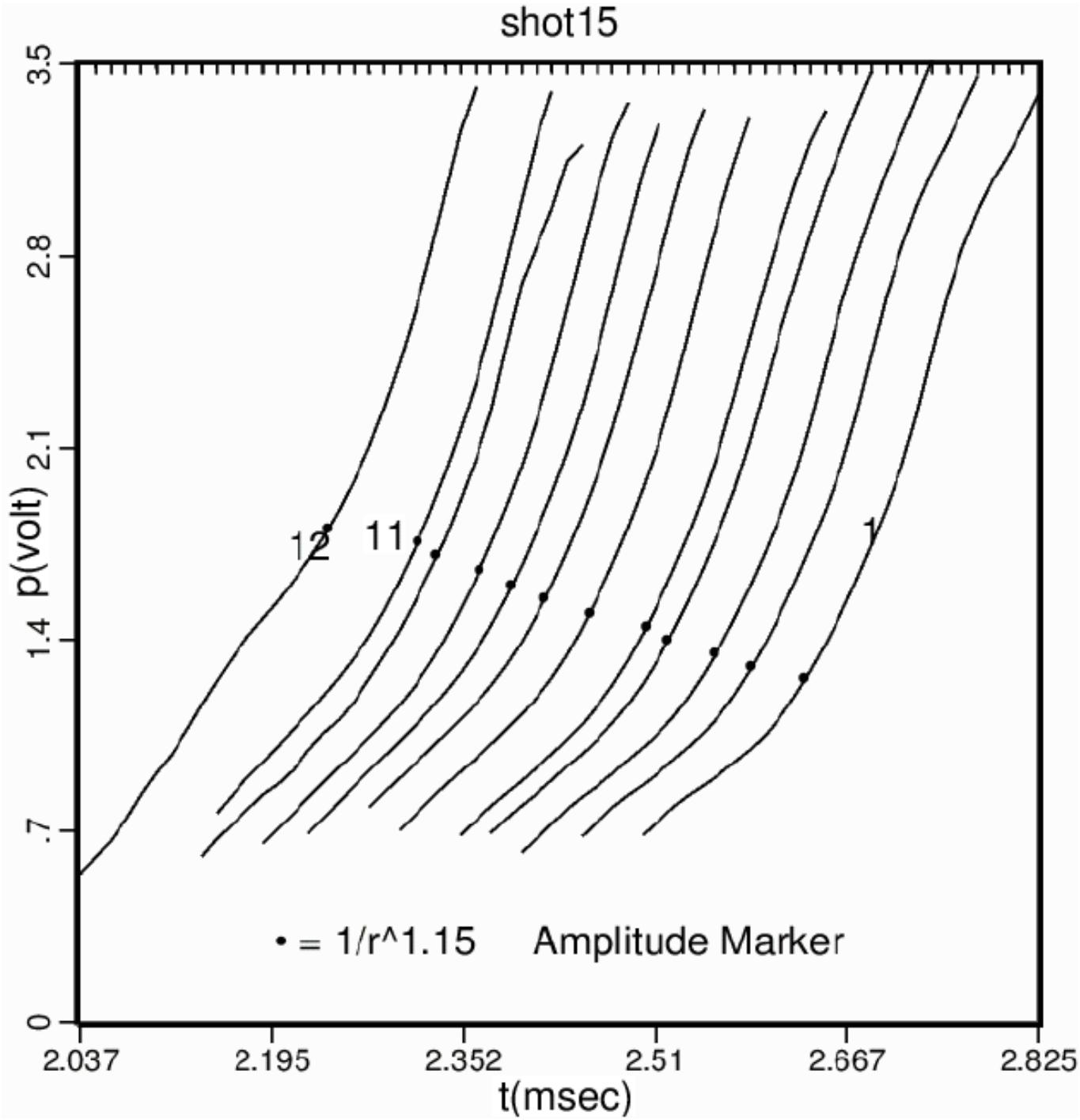

Figure 7. Amplitude marking scheme for pressure- time series motivated by Fig. 4. Hydrophone pressure is expressed in volts, with conversion 10kPa/v.

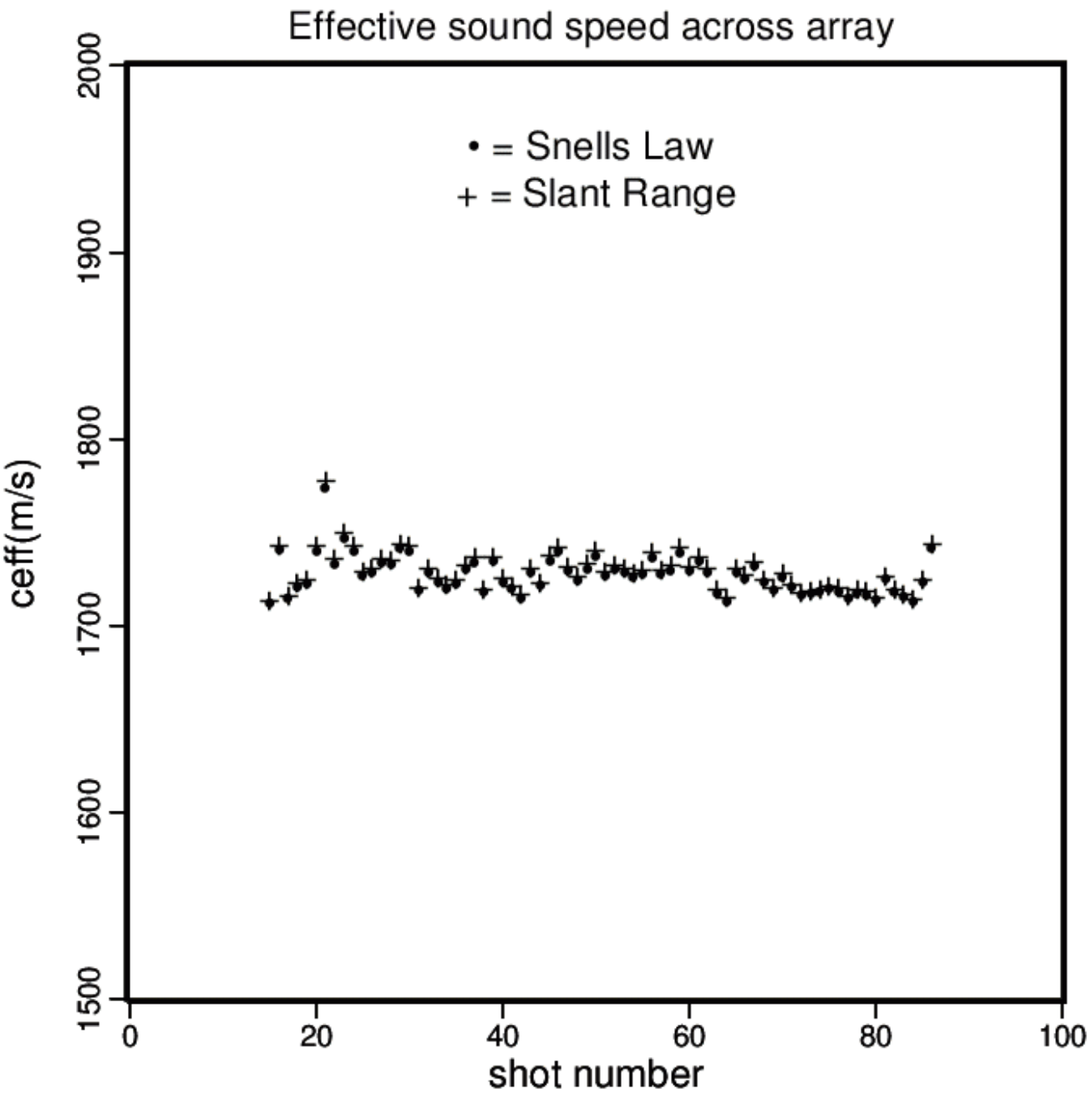

Figure 8. An example of the amplitude marking scheme for determination of *in situ* sediment sound speed using eq. (22). Dots: ray paths from Snell's law; + signs: straight ray paths with no deflection at the seafloor.

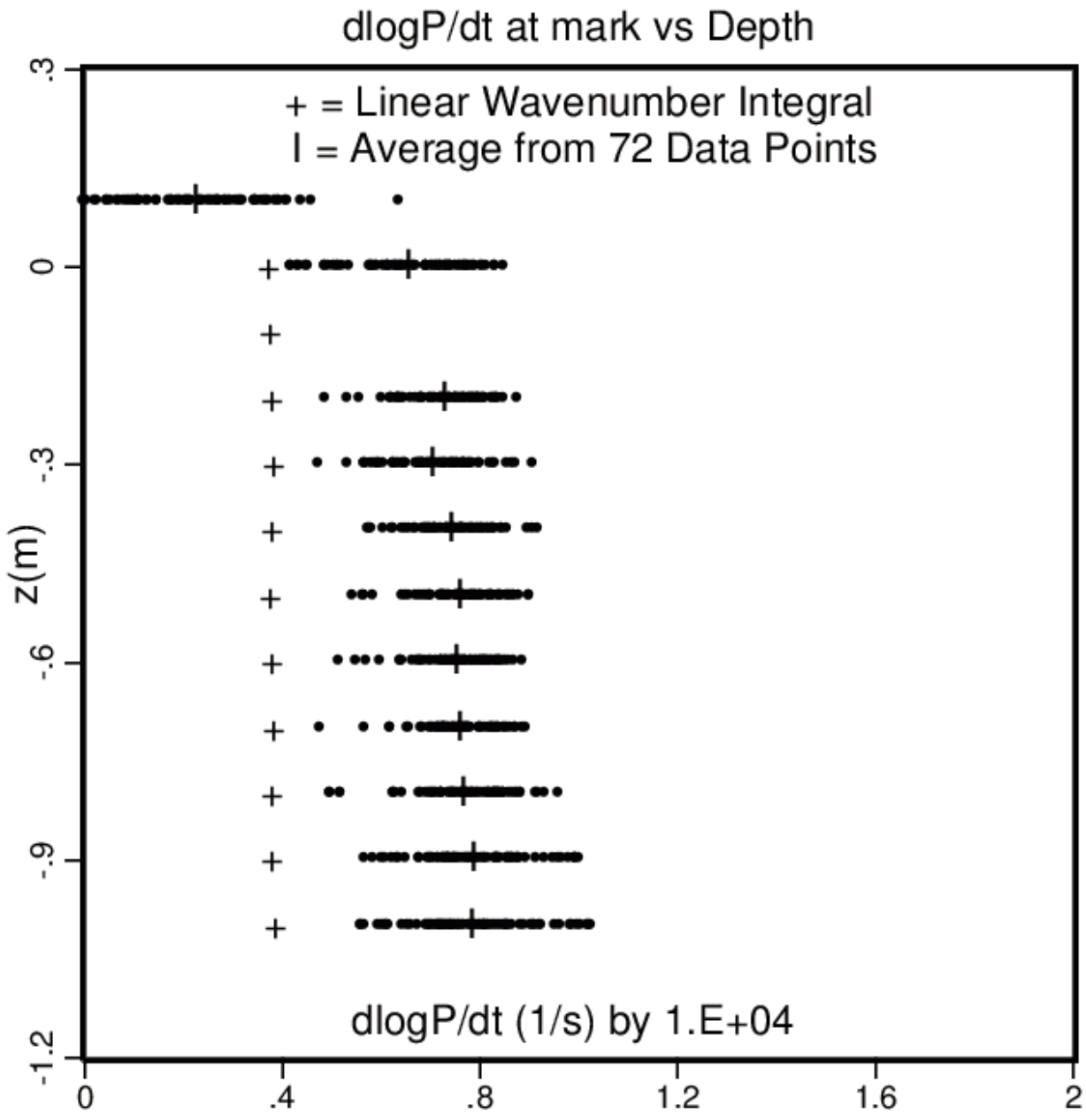

Figure 9. Log- pressure time derivative at marker locations at each array element (phone 10 was defective). Dots: individual data from 72 shots. Vertical bar: Data averaged over 72 shots. Plus sign: Linear broadband wavenumber integral from eq. (14) integrated over 1 - 1800 Hz illustrating near constancy of the log- pressure time derivative.